

Surface integrity of hybrid CM247LC/Inconel 718 components produced by laser-directed energy deposition

MEHMETI, Aldi <<http://orcid.org/0000-0001-7192-5543>>, BIDARE, Prveen, IMBROGNO, Stano, WIMPENNY, David, ESSA, Khamis and DIMOV, Stefan

Available from Sheffield Hallam University Research Archive (SHURA) at:

<https://shura.shu.ac.uk/33287/>

This document is the Published Version [VoR]

Citation:

MEHMETI, Aldi, BIDARE, Prveen, IMBROGNO, Stano, WIMPENNY, David, ESSA, Khamis and DIMOV, Stefan (2022). Surface integrity of hybrid CM247LC/Inconel 718 components produced by laser-directed energy deposition. *The International Journal of Advanced Manufacturing Technology*, 121 (7-8), 4961-4980. [Article]

Copyright and re-use policy

See <http://shura.shu.ac.uk/information.html>



Surface integrity of hybrid CM247LC/Inconel 718 components produced by laser-directed energy deposition

Aldi Mehmeti¹ · Prveen Bidare¹ · Stano Imbrogno² · David Wimpenny³ · Khamis Essa¹ · Stefan Dimov¹

Received: 18 May 2022 / Accepted: 23 June 2022 / Published online: 13 July 2022
© The Author(s) 2022

Abstract

High-temperature alloys pose significant challenges in additive manufacturing. These materials have unique properties, such as high resistance to mechanical and chemical degradation when exposed to high temperatures. Furthermore, when these alloys are used to produce hybrid components with other similar alloys, investigating their surface integrity is critical because any residual stress can lead to early stage cracks and poor fatigue performance. In this research, a hybrid manufacturing approach is employed to produce components from difficult to weld alloys, i.e. CM247LC deposited on IN718 through a laser based direct energy deposition (L-DED) process. The surface integrity, mechanical properties and microstructure of such hybrid components is investigated, especially their welding/joint areas. Crack-free processing regimes were established to deposit CM247LC while mitigating the negative effects onto the microstructure of the Inconel substrate. Especially, the thermal gradients were managed to deliver crack free sections of CM247LC with good interface bonding, strength and fine microstructure. It is important to note that this is achieved without any significant preheating that contrasts with what is reported in other investigations so far. Furthermore, end-use hybrid blisks with deposited CM247LC blades onto Inconel 718 disks (HUB) were manufactured and then machined within a single processing set-up. The results show that the substrate thickness, the machining between the deposited layers and the final machining and heat-treatment play a role in reducing residual stresses. Ultimately, such hybrid manufacturing approach can be considered a new solution for producing such components and also for their subsequent repair.

Keywords Additive manufacturing of CM247LC/Inconel718 · Surface integrity of hybrid components · Bonding interface · Residual stresses · Mechanical properties · Microstructure observation · Hybrid blisk

1 Introduction

Compressors and fans are key components of modern aero and gas turbine engines. High-pressure (HP) turbine blades are exposed to severe operating conditions [1], such as fatigue loadings, temperature and corrosion that often lead to cracks and may cause catastrophic failures of the engines [2]. Therefore, such critical components have to be produced from high temperature alloys, specially developed

for such applications [3, 4]. These are typically nickel-based superalloys, i.e. CMSX-6 [5], DZ125 [6], Inconel 718 [7] and CM247LC, chosen due to their superior mechanical and physical properties. CM247LC is a well-known material for such application because of its excellent pitting resistance and superior mechanical properties under high thermal loads [8]. However, the manufacture of components with complex geometries from CM247LC and Inconel 718, too, is very challenging and cost prohibitive when traditional processing technologies are employed, due to their intrinsic limitations [9–15].

Recently, additive manufacturing (AM) processes, such as laser powder bed fusion (L-PBF) and laser direct energy deposition (L-DED), have attracted a significant industrial interest, especially for producing complex geometrical components, e.g. parts with conformal cooling channels and internal features, while offering resource efficiency and environmental sustainability. The L-DED technology

✉ Aldi Mehmeti
axm1451@student.bham.ac.uk

¹ School of Mechanical Engineering, University of Birmingham, Edgbaston, Birmingham B15 2TT, UK

² School of Metallurgy and Material Sciences, University of Birmingham, Edgbaston, Birmingham B15 2TT, UK

³ MTC, Ansty Park, Coventry CV7 9JU, UK

can be employed both for producing new components and for their repair, and thus to extend their lifespan. Despite these advantages, the processability of nickel alloys, such as Inconel 718 and especially CM247LC, is still a challenging task and therefore is the focus of a significant research interest. Primarily, due to the poor weldability of the material and its susceptibility to cracks that are the result of the high γ' fraction, especially the side effect of reheating and remelting of layer-wise processing strategies in AM [16, 17]. Additionally, the build rates achievable with the AM technologies are relatively low [18] and near net shape parts are produced that require post-processing to meet the surface integrity and accuracy requirements of any give application [17, 19, 20]. Also, the existence of metallurgical defects, i.e. residual stresses, various types of cracks, such as solidification, liquation ductility dip cracking (DDC) and internal porosity due to unmelted powders and gas entrapment, can significantly impair the mechanical properties of the parts [21–25]. Ultimately, this is a standalone process that is difficult to integrate with any necessary pre- and post-processing technologies in existing conventional manufacturing systems. In general, L-DED parts have significant limitations regarding their surface integrity and mechanical properties. Therefore, they are usually not considered a suitable option for safety-critical applications.

The recent trend in the turbine blades development is a single unit design, i.e. the disk (HUB) and blades are produced as one piece that is often referred to as blisks [26]. Such complex components can be produced employing different manufacturing technologies, such as machining, laser cladding and additive manufacturing [27], followed by hot isostatic pressing and thereafter are machined/finished through subtractive process, i.e. milling, to meet demanding surface integrity and geometrical accuracy requirements [18, 28–30].

It could be stated that all processes used for the manufacture of turbine blades/blisks have some limitations. Therefore, their capabilities are usually combined into manufacturing platforms to meet the constantly growing requirements for blades and blisks production [31]. The most novel and flexible production solutions combine two or more manufacturing technologies sequentially, referred to as hybrid manufacturing systems or processes [18, 32]. Some state of the art systems combine L-DED process synergistically with subtractive ones, i.e. machining, into hybrid machine tools such as LASERTEC 65 3D from DMG Mori [33, 34]. Lately, researchers reported a new methodology for automatic ultrasonic testing (UT) of LMD-powder additively manufactured preforms with the feasibility of detecting and locating surface and internal defects [35].

Although the L-DED process is considered suitable for producing complex components for aero-engines or energy applications, it has some important limitations. As a layer-based manufacturing process, the build component undergo multiple thermal cycles that can lead to weld stresses and microstructure changes of the processed material, especially when CM247LC is utilised [36]. The high thermal gradients and fast cooling rates between the deposited layers introduce additional residual stresses to those induced due to γ' strengthening phase. Thus lead to an internal strain that exceeds the material ductility and triggers crack formation [37, 38]. Researchers had already reported induced cracks due to residual stresses in L-DED CM247LC parts, although, the investigation was limited to the microstructure changes of single pass thin wall structures and their heat treatments while the residual stresses were not studied [8, 39, 40]. Furthermore, the studies were conducted in an inert gas environment, i.e. argon and/or by employing auxiliary energy source coupling (induction) to achieve a better thermal control and tailoring during the CM247LC deposition [8, 41, 42]. Although the processing of these difficult to weld material has attracted a significant research interest, very few results have been reported on producing hybrid structures that combine wrought Inconel 718 with L-DED CM247LC [1, 41]. Therefore, more research is required that is focused on investigating the surface integrity, mechanical properties and microstructure of the hybrid sections, especially their welding/joint areas. A continuous pre-heating at temperatures between 1050 and 1100 °C to control the CM247LC solidification cracking at the temperature ranges reported in literature could have a significant negative impact onto the Inconel 718 microstructure, when depositing structures on Inconel 718 substrates/preforms, therefore was not considered in this study [41, 42]. Consequently, alternative regimes are investigated in this work to deposit crack free CM247LC structures while mitigating any negative effects on Inconel 718 microstructure.

To the best of the authors' knowledge, there is no research reported on surface integrity of hybrid components produced by depositing CM247LC on Inconel 718 substrates. Therefore, this research is focused on investigating residual stresses at the joining areas of such hybrid components. By applying the proposed approach to control the thermal gradients during L-DED in this research, it was possible to produce crack free CM247LC structures with good interface bonding, strength, and microstructure for as built and heat-treated conditions. Furthermore, a feasibility study on producing hybrid blisks by depositing CM247LC on wrought Inconel718 disks (HUB) was conducted in single processing setup that integrates L-DED with milling. The next section introduces the materials and methods used in the research and then the results are discussed, and conclusions are made.

Table 1 Material composition (% by mass)

CM247LC													
C	Al	Ti	Cr	Mo	Hf	Ta	Co	W	B	N	O	O (supplier)	Ni
0.09	5.57	0.80	8.29	0.61	1.31	3.10	9.59	9.57	140 ppm	<20 ppm	<100 ppm	75 ppm	Bal
Inconel718													
C	Al	Ti	Cr	Mo	Nb	Fe	Co	Cu	B	N	O	O (supplier)	Ni
0.023	0.48	0.97	18.15	2.97	5.15	18.35	0.39	0.04	140 ppm	<20 ppm	<100 ppm	0.00003	Bal

2 Materials and methods

2.1 Materials and fabrication methods

A gas atomised CM247LC powder supplied by Carpenter Additive was employed in the manufacture of hybrid structures and the chemical composition of the material is provided in Table 1. As shown in Fig. 1, the particles are spherical with some fine and satellite ones. The average particle size, d_{50} , is 63 μm .

Inconel718 substrates in their annealed state (A79706) were used and their chemical composition is shown in Table 1, too. The L-DED process was performed initially on planar Inconel 718 substrate and thin walls were produced to determine parameters domain that was used in the subsequent deposition trials and also in the feasibility study on the manufacture of hybrid blisks. The L-DED parameters used were as follows: laser power 800 W, scan speed 240 mm/min and powder flow rate of 9.8 g/min. More information about the selected process parameters is provided in another study [43].

Both alloys used in the research were selected because they are widely used by industry for the manufacture and/or repair of aircraft components. The L-DED trials were conducted on a commercially available hybrid 5 axes machine tool, i.e. Mazak Integrex i400AM [44].

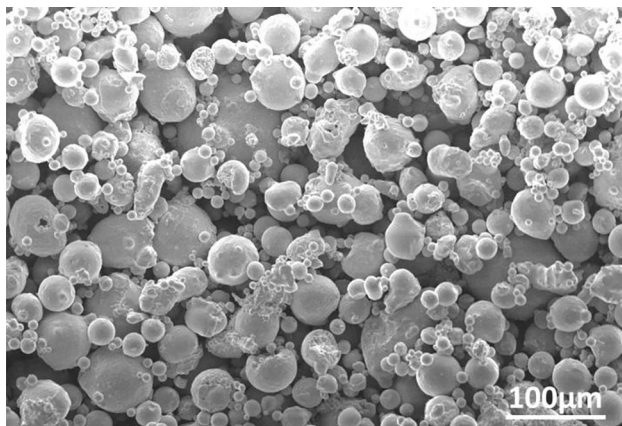


Fig. 1 A SEM image of the CM247LC powder used in the experiments

This is a multitasking system that integrates machining and L-DED technologies in a single processing setup. The hybrid machine tool utilises a coaxial nozzle as shown in Fig. 2, and standard tool holders are used to execute the L-DED operations and a range of machining tasks in the same processing setup. Thus, it is possible in this hybrid machine tool to pre-process Inconel 718 substrates and then to machine/finish the deposited CM247LC structures without any re-setting of the hybrid workpiece. A continuous wave (CW) near infrared (NI) laser source from IPG Photonics with average power of 1 kW is integrated into the hybrid machine tool to realise the L-DED operations. The AMBIT high-rate deposition head from Hybrid Manufacturing Technologies was used, while, a beam spot size of 2 mm was achieved through a 10 mm standoff distance.

The hybrid samples were produced to carry out an analysis of their residual stresses, further information about them is provided in the supplementary material to this work (see the Appendix). The CM247LC deposition was conducted in the open chamber of the hybrid machine tool and argon gas through the deposition head was used to shield the area around the beam spot. Thus, the produced samples can be considered representative of CM247LC structures and hybrid parts that can be manufactured using commercially available

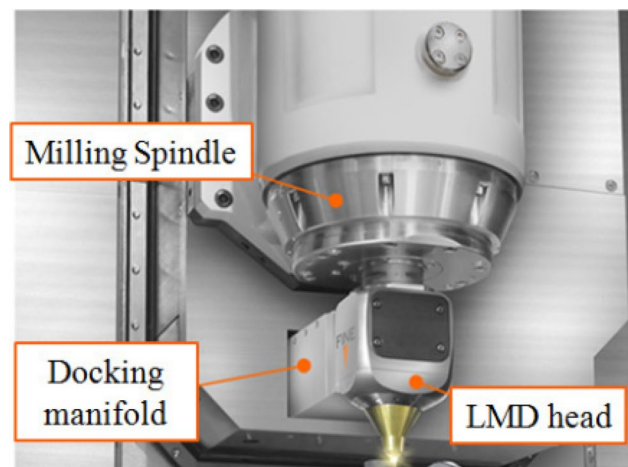


Fig. 2 The deposition head used to execute L-DED and machining operations in a single processing setup [44]

processing setups. It is important to stress that the hybrid machine tool does not have any additional process monitoring tools and/or auxiliary heating elements to minimise the negative side effects in welding Ni-based super alloys, especially to suppress their high cracking susceptibility. The delta fraction at 1060 °C decreases to 0% within minutes and thus its retardation effect onto the crack propagation and creep-rupture resistance decreases quickly, especially in well oriented plate like structures as those in forged billets extensively used to produce disks [26, 45]. So, the use of induction heating at temperatures ranging from 1050 to 1100 °C was not considered, as recommended in other investigations [41, 42] and a specially designed regime was developed to produce the CM247LC structures in this work. Especially, multilayer sections with unidirectional depositions and height of ~4 mm are produced sequentially and before the deposition continues with processing strategies rotated at 180° as shown in Fig. 14(b), a dwell time of 45 s between them is applied, as suggested by other researchers [46, 47].

A standard heat treatment was applied, too, in this research that included three steps as proposed by other researchers [8, 48]. The steps of this heat treatment are summarised in Table 2. The temperature of the solid solution step was selected to homogenise the γ' -precipitates of deposited CM247LC. Thus, it was above the solvus temperature of undesired Laves phase in the Inconel 718 substrate and also the dwell was long enough to dissolve it. This step is then followed by the double-ageing heat treatment required to grow the desired strengthening phases and so to harden the material. The heat treatment was applied only to a set of samples that required some further machining.

2.2 Characterisation methods

Characterisations were applied on three hybrid specimens from each state. The following characterisation steps and tests were employed to study the microstructure and surface integrity of the hybrid specimens:

➤ *Optical microscopy and scanning electron microscopy (SEM) analysis.* A metallography analysis of hybrid components was conducted to investigate the microstruc-

tural evolution before and after the heat treatment using Hitachi TM3030 SEM system with integrated backscatter (BSE) and energy-dispersive X-ray spectroscopy (EDS) detectors.

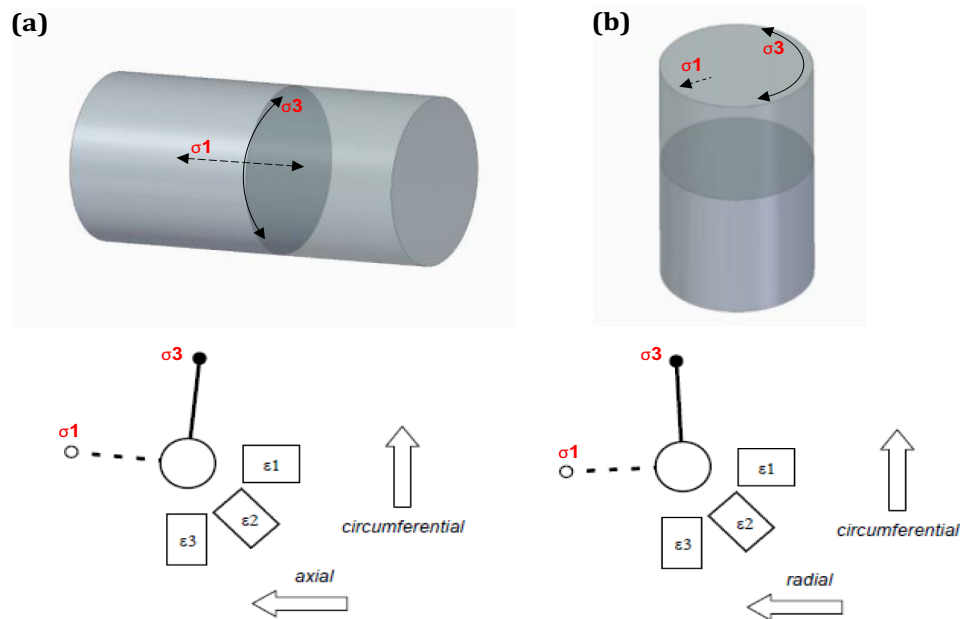
➤ *Hardness analysis.* The bonding between Inconel 718 preforms and the deposited CM247LC structures were analysed. The analysis included a set of two successions of ten Vickers indentations at 0.6 mm from the interface into the machined preform and 0.5 mm into the deposited structures, with a load of 0.3 kgF for 12 s.

➤ *Residual stresses.* Residual stresses were analysed employing the target gauge/centre hole drilling method (ASTM E837 (2013) standard) by Stresscraft Ltd. The residual stresses have been determined based on relaxed strain measurements to a maximum depth of 1024 μm . Strain gauges were positioned at two locations of each hybrid sample. Especially, one gauge was placed at the substrate, ~1.2 mm below the interface, and the second at the deposited structure approximately at 50% of the diameter of the sample. Each sample was cemented to an angle plate fixed to a drilling rig for alignment with the miniature 3 axis drilling setup. The attached gauges were aligned parallel to the build direction (0°) and perpendicular (90°) to the build direction at the XY plane. Orbital holes were drilled with depth increments set to $4 \times 32 \mu\text{m} + 4 \times 64 \mu\text{m} + 8 \times 128 \mu\text{m}$ to give a final depth of 1.408 mm, the stress data was generated to a depth of 1024 μm . The anisotropic Young modulus of deposited CM247LC, i.e. 159.2 GPa with a Poisson's ratio of 0.3, was employed in this assessment, as per ASTM E387. The axial/radial (σ_1) and circumferential (σ_3) stresses with their respective directions are shown in the diagram in Fig. 3. The aforementioned values were taken from the measurements of as built additively manufactured samples [49]. While for the Inconel718 substrate, the corresponding values were 200 GPa and 0.29, for the elastic modulus and Poisson's ratio, respectively. The reported values were acquired by Stresscraft Ltd.

Table 2 The applied heat treatment with its respective steps, temperatures and holding times

Cycle	Solution	1st Aging	2nd Aging
Temperature	1260 °C	705 °C	621 °C
Holding time	2 h	10 h	20 h
Approx. cooling rate	Rapid cooling in air	Furnace cooling to 621 °C	Rapid cooling in air

Fig. 3 Schematic representation of σ_1 (axial/radial) and σ_3 (circumferential) stresses direction for each gauge installation: **a** gauge installation location at interface; **b** gauge installation location at L-DED section (ϵ denote strains)



3 Results and discussion

3.1 Residual stresses

3.1.1 Residual stresses at the interface

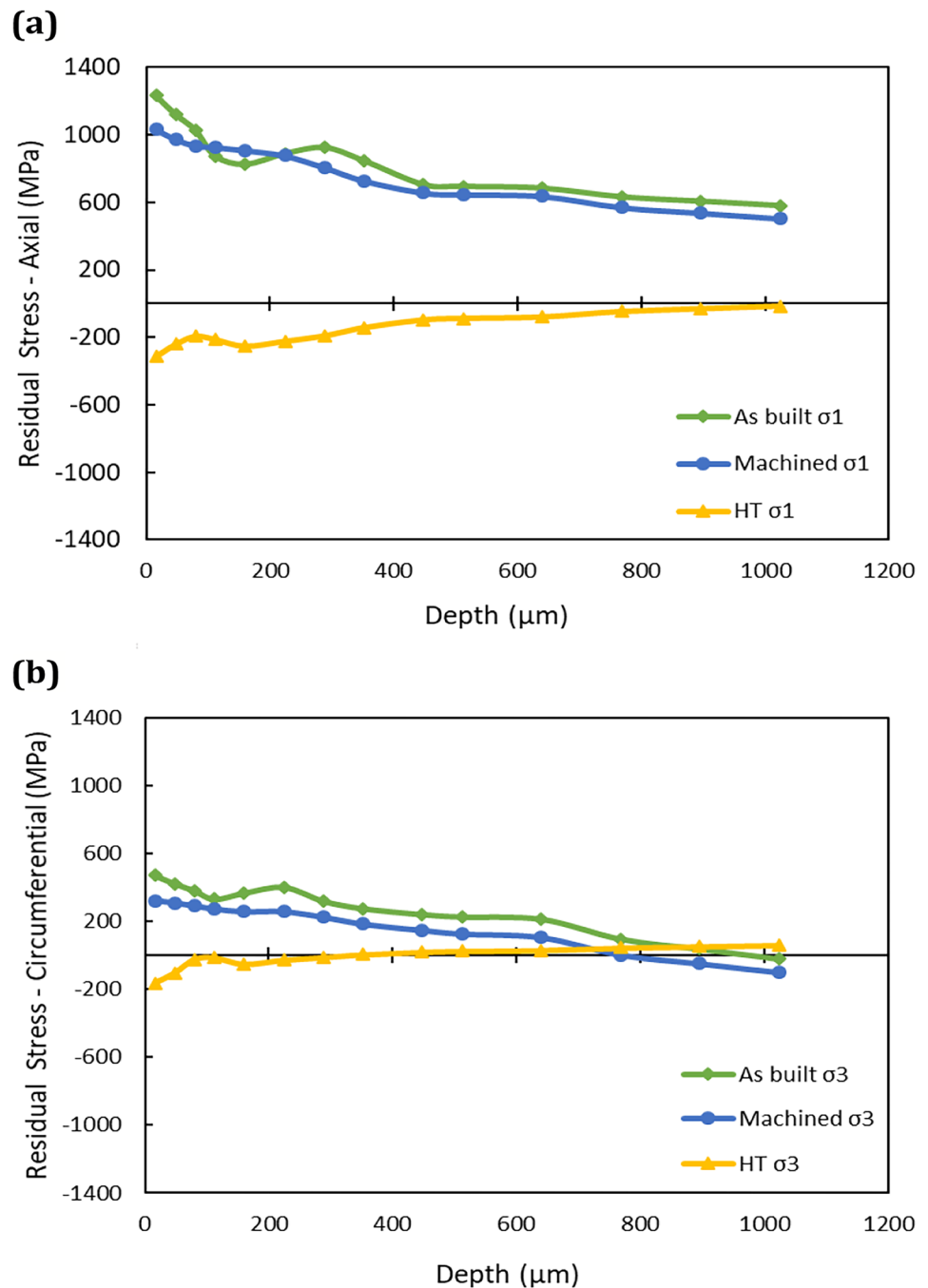
The axial stresses at the interface section of the hybrid cylindrical specimens showed a peak value of 1233 MPa in the as-built state, 1035 MPa for the intermediate machined state and -314 MPa for its heat-treated state at a depth of 16 μm of the σ_1 (axial) stress distribution. Conversely, the respective near surface circumferential stresses of the as-built specimen and the machined one were 471 and 323 MPa, respectively that were significantly lower compared to their σ_1 stresses. For both specimens, the stresses decreased with the depth over the range of assessments to 583 MPa and 504, respectively, while the σ_3 stresses appeared to be compressive.

Apparently, there is a significant difference between the σ_1 and σ_3 stress distributions, especially for the as-built and machined specimens. It is evident that the stresses in the σ_1 direction are tensile compared to σ_3 at all depths. Moreover, the tensile stress decreased rapidly in the σ_3 direction and tends to be compressive at $\sim 900 \mu\text{m}$. In addition, the thickness of the layer affected by the tensile stresses is higher in the σ_3 direction of the as-built specimen, i.e. 896 μm , while the stresses are neutral in the machined specimens at a depth of $\sim 750 \mu\text{m}$. This phenomenon is attributed to the distribution of residual stresses in the preform after the additive and subtractive processes. Although the interface at the Inconel 718 preform was machined prior to the deposition and therefore the stresses are expected to be compressive due to the nature of the machining process [50], this is not the case as it

can be seen in Fig. 4. The stresses are tensile with peak values higher than 1000 MPa in the build direction. These tensile stresses can be attributed to the intrinsic reheating and remelting during the additive process where the heat from the laser source reduces the initial compressive stresses after the machining. This relaxation of the compressive stresses continues as the height of the deposited material increases. Especially, the deposited material constrains the previously deposited layer, so the plastic deformation occurs for longer and consequently the initial tensile stresses increase. Thus, the initial tensile stresses would increase due to the thermal stress with the increase of deposited material, while the compressive stresses induced during the machining remain unchanged. Thus, the final residual stresses quotient at the interface are tensile. These tensile stresses decrease with the increase of deposited material as reported by others, too [51, 52]. This explains to some extent the concentration of excessive stresses at the interface.

The energy penetration from the laser source had a significant impact on the vanishing of the beneficial compressive stresses after the initial machining. Therefore, it is apparent that the heating from laser irradiation has had substantial effects into the Inconel 718 preform and thus it can be stated that the surface preparation process, such as machining or grinding, has a limited or marginal effect on residual stresses into the deposited material [53]. In particular, the heat affected zone at the interface triggers a redistribution of dislocation densities that consequently affects the sub-surface below the high shear zone of the machined material, as shown in Fig. 4a. The microstructure alternation into the Inconel 718 preform is present up to a depth higher than 450 μm , which suggests the substantial changes because of

Fig. 4 The stress distribution at the interface: **a** axial stresses (σ_1) distribution in depth for all material conditions; **b** the distribution of circumferential stresses (σ_3) in depth for all material conditions



the material re-melting at the interface. This is also evident from the hardness test results where the obtained similar values indicate some microstructure homogenisation at the interface. As the substrate did not show any distortion at the interface, it could be assumed that no stress relaxation occurred due to annealing and also this could be attributed to the preform preheating prior to the CM247LC deposition [54]. Furthermore, it is evident that the pre-heating and the interlayer dwell reduce the residual stresses, as they are known to be proportional to the thermal gradients between

the ambient and melting temperatures [55]. Additionally, as there was no delamination or separation at the interface, it can be stated that both remedies were adequately chosen to manage the residual stress development.

Any surface preparation stages, e.g. texturing or machining of preforms, had no effect on the bonding performance after the material deposition [56]. This can be explained with the laser irradiation effects that are dependent on the laser type employed in the L-DED process and its intrinsic parameters [21]. The CW laser has been reported to induce

significant fluid flow, such fluid flow patterns normally occur due to a gradient of surface tensions at the interface between the two molten materials that is referred to as Marangoni effect [57]. A positive thermocapillary gradient achievable with the CW lasers stimulates the Marangoni convection and can lead to a higher penetration depth between the Inconel 718 preform and the deposited material when compared with the effects of pulsed lasers [58–60]. Overall, a CW laser processing is observed to lead to a deeper penetration into the substrate material, as shown in Fig. 15 (see Appendix), which is in line with the results reported in [58–60]. Therefore, it can be stated that the manufacture of hybrid components by employing CW lasers in the L-DED process has a beneficial effect as the penetration depth is crucial for the microstructural assimilation and bonding at the interface between the two materials. Especially, this is the case when structures have to be deposited on thick preforms/substrates, such as the disks of the blisks, or a small volume of material should be deposited in repair applications, where the microstructural bonding is crucial.

It can be stated that the axial stresses of the heat-treated (HT) specimen remained compressive at all depths up to 1024 μm , while circumferential stresses showed a peak of 60 MPa. Indeed, the HT cycle had a positive impact and reduced the maximum tensile stresses at the interface in both σ_1 and σ_3 directions and contributed to the transformation of the tensile stresses into compressive (see Fig. 4), as also reported by Barros et al. [61]. The HT regime delivered mainly compressive stresses of almost 300 MPa in both directions. Thus, it can be stated that HT is very important for the formation of compressive stresses at the interface in σ_1 and σ_3 directions. Therefore, such solution treatment should be considered mandatory for the relaxation of tensile stresses, annealing, including precipitates and dislocation networks along the sub-grains, and so to dissolve segregations and precipitates at the grain boundaries as suggested by [62].

3.1.2 Residual stresses of the L-DED section

For the as-built and the HT deposited section, the near surface σ_1 and σ_3 stresses are compressive as can be seen in Fig. 5. The compressive stresses can be attributed to the smoothing process (site preparation) applied at the two sites for the installation of the gauges. Nevertheless, such stresses do not appear to penetrate to depths higher than 100 μm . The σ_3 maximum stresses at 160 μm are 319 and 46 MPa for the as-built and the HT specimens, respectively. The corresponding radial stresses were 97 MPa and 28 MPa, respectively. At the maximum depth 1024 μm , the σ_1 and σ_3 stresses were 39 MPa and 38 MPa and 184 MPa and 21 MPa, for the as-built and HT specimens, respectively.

These tensile stresses can be attributed to reheating and remelting cycles during the L-DED process, i.e. the layer-based deposition processes. Especially, the newly deposited material constrains the previously deposited layer and so the plastic deformation is sustained for longer and thus increases the initial tensile stresses of as-built samples. The circumferential σ_3 stresses (scanning direction) are larger than the radial σ_1 stresses, and this could be explained with the higher contraction of the heated material in the respective direction [52]. Particularly, the stresses in the scanning direction are almost twice higher than those observed in the radial one. Again, this result can be attributed to the thermal shrinkage of the solidified layer and is consistent with the results reported in other studies and thus the methodology used in this research can be considered valid [55].

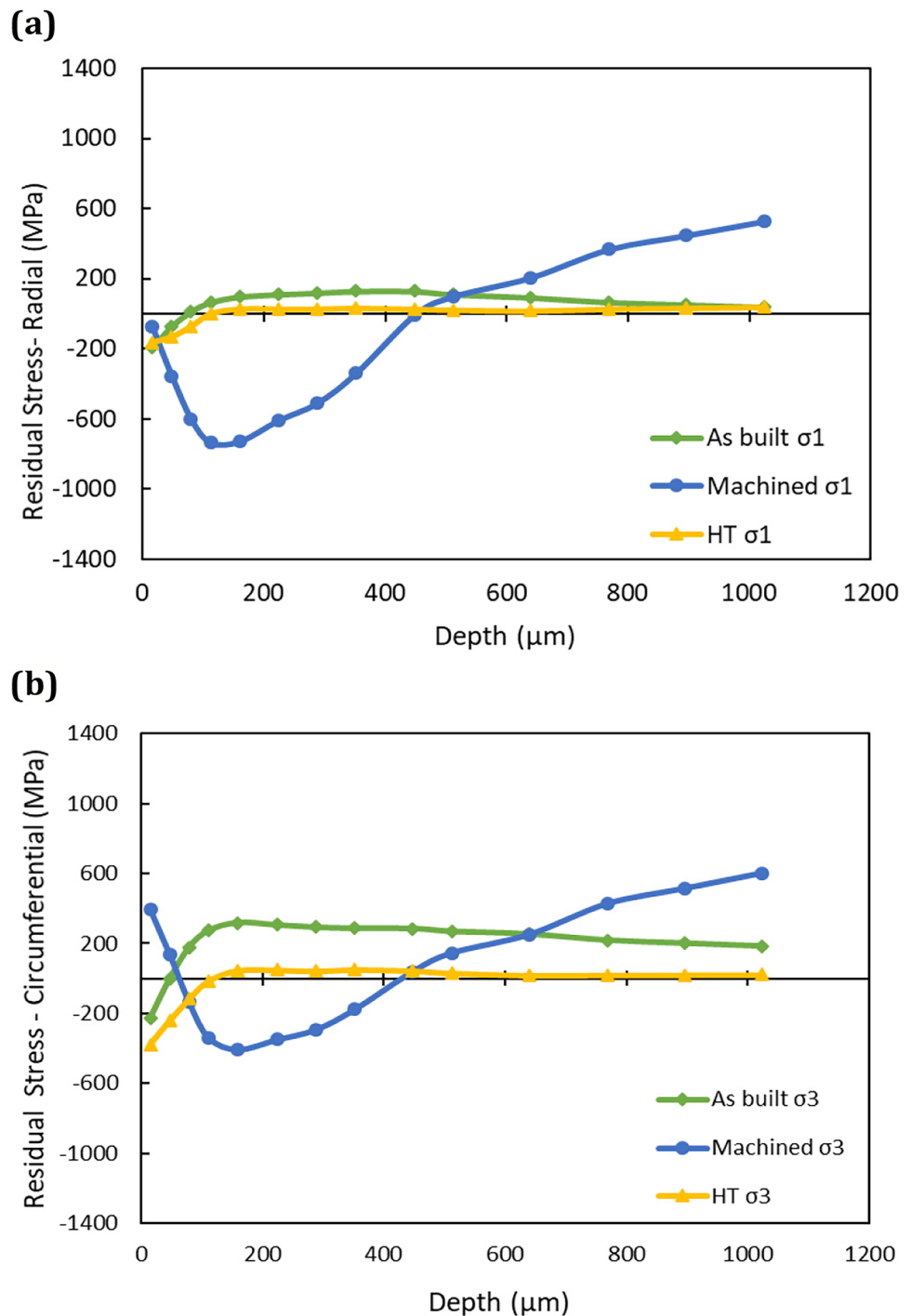
Notably, the peak value of tensile stresses obtained for the as-built specimens is significantly lower than those reported in the literature for as-built CM247LC [49] and lower than the yield stress for cast CM247LC [63]. The low peak values can be attributed to the inter-layer delay applied in the deposition strategy used in this study. A similar approach was reported by Denlinger et al. [64] that used inter-layer dwelling to minimise residual stresses on deposited Inconel 625 structures, while Fessler et al. reported that by using dwell between L-DED layers reduces the distortion when depositing Invar [65].

In line with previous findings, the solution HT at the selected temperature induced relaxation of tensile stresses at the deposited structures. The mechanism, formulation details and additional benefits from the solution HT are explained in the literature [62].

For the machined specimens, the stresses were found to be dominated by those generated by the machining process. The radial direction is along the feed motion while the σ_3 direction to the cutting speed direction. Figure 5b shows the higher residual stresses in the circumferential direction and they were found to be higher than those in the radial direction. This can be attributed to the high plastic deformations induced by the cutting tool, during the machining process. These results are in line with those reported in the literature [50].

The first measurements for the machined specimen were –73 MPa for σ_1 and 395 MPa for σ_3 . Then, the stresses decrease with the increase of the depth, initially, and reached their minimum values at a depth of 160 μm . The stresses at this depth were –728 MPa and –405 MPa, for σ_1 and σ_3 , respectively. Next, the stresses for both σ_1 and σ_3 increased to reach the maximum values of 528 MPa and 603 MPa at 1024 μm , respectively. The overall stress distribution for the machined sample is typical for such samples, as the very large forces induced during machining at low cutting speeds lead to higher plastic deformations and a greater impact on the residual stresses [66]. The affected areas are

Fig. 5 The stress distribution in the deposited sections: **a** radial stresses (σ_1) distribution with depth for all material conditions; **b** circumferential stresses (σ_3) distribution in depth for all material conditions



expected to show slip bands and dynamic recrystallisation due to the thermal and mechanical loads induced during the machining process [67]. Especially, the balance between the thermal and mechanical loads determines the nature of the stresses in the bulk [68]. As the investigated material is a heat restraining material, the thermal load is reported to be greater than the mechanical load, therefore triggering tensile stresses. The depth of the layer affected by the tensile stresses is larger for the as-machined specimens in both σ_1

and σ_3 , compared to HT ones. This is similar to the neutral stresses in both directions at a depth of 600 μm that can be explained with ductility of the material being machined prior the solution HT.

The machined sample demonstrates significantly high compressive stresses up to a depth of 450 μm that then decrease in both σ_1 and σ_3 directions. This is mainly due to high deformations, as the area is a high shear strain zone (HSSZ) [67]. Thereafter, this effect fades away and the

stresses become tensile as per the as-built sample. This conforms to the initial results reported in the previous section regarding the fusion zone depth. This has been observed in other studies, too, where the presence of tensile stresses is common in as-built L-DED parts and therefore explains the spike in tensile stresses due to the HSSZ zone induced by the AM process [69]. Although, machining exhibits substantial benefits by introducing compressive stresses, it is important to note that the machining parameters were not optimised in this study.

Comparing the stress values obtained in this work with those reported in literature, it can be stated that it is beneficial to apply dwell and thus to minimise the residual stresses significantly below the yield strength of CM247. Subsequently, if the effects of the inter-layer dwell are compared to those of intermediate machining, it can be noted that its effect on reducing the stresses is marginal. This phenomenon can be attributed to the initial tensile stresses, and the subsequently introduced thermal stress increase with the newly added layers, while the compressive stresses induced from the machining remain unchanged. Therefore, the final residual stress quotient, in the bulk of the material, is tensile. Ultimately, an intermediate machining of the AM structures reduces only marginally the residual stresses at the interface. Naturally, by introducing intermediate machining at a higher frequency would potentially reduce the overall stresses, correspondingly. Nevertheless, multiple machining passes for the investigated materials, come at a cost and may not be viable for a given application [10]. To investigate the failure of the interface due to peak stresses, the Von Mises theory was employed to understand the failure mode, as the Inconel bar substrates area relatively ductile.

Peak stresses were calculated based on the principal σ_{\max} and σ_{\min} , stress values. The Von Mises (VM) stresses in Inconel are calculated as follows:

$$\sigma_{vm} = \sqrt{(\sigma_{\max}^2 + \sigma_{\min}^2 - \sigma_{\max}\sigma_{\min})} \quad (1)$$

The peak values for VM stresses of the as-built interface was 1264 MPa while the machined and HT ones had peaks of 1168 MPa and 351 MPa, respectively. Thus, for the as-built and machined interfaces, the VM stresses are substantially greater than those after solution HT.

The maximum VM stresses obtained for the as-built interface are marginally higher than the yielding stress (YS) of the material, $YS_{0.2} = 1220$ MPa, but the substrate section does not show any signs of distortions or cracking. The marginal deviation could be related to the strain gauge measurements, which could be affected by the plastic deformations during the orbital drilling, and thus are likely to affect the obtained results [49]. However, this should not be considered conclusive as the intermediately machined sample demonstrated a similar high peak value, although below

the material maximum limit and thus an additional investigation is required. The intermediate machining passes are found to have contributed marginally to the reduction of the maximum tensile stresses. Especially, they break the initial stress equilibrium introduced from the deposition process as discussed earlier in this section. Subsequently, this had an impact on the overall reduction of the VM stresses.

As the deposited CM247LC is found to be a material with a limited elongation [8], the maximum principal theory is used. According to the theory, failure occurs when the maximum principal stress reaches the ultimate stress of the material. For the as-built condition, the maximum principal stress was 336 MPa at a depth of 160 μm . Apparently, this maximum principle stress is lower than the UTS and YS reported in literature for L-PBF, L-DED and cast CM247LC, respectively [8, 39, 63].

Contrasting the as-built condition to that of the intermediate machined sample, the peak value was 604 MPa, at a depth higher than 1 mm, although with a tendency to increase with the depth. While the HT sample showed a peak of 51 MPa, it was well within the range of the ultimate strength of the material.

Even though the fatigue life of hybrid components was not investigated in this research, it can be stated that the deformations and residual stresses induced by machining and machining follow up by HT can have a substantial impact on the fatigue behaviour of the materials, especially by increasing their fatigue life [70]. Therefore, the stresses distribution induced by the finishing operations, such as machining and solution HT, can potentially enhance the performance of the hybrid components in regard to their fatigue life.

3.2 Process development

The hybrid manufacture of a blisk-like test part was attempted based on the acquired results. The pilot manufacture was performed on the same hybrid Mazak Integrex setup used for the residual stresses result reported in Sect. 3.1. As this is a commercially available machine tool, this feasibility study aims to inform potential industrial applications about the viability of the proposed hybrid solution, especially where small and medium batches of hybrid components have to be produced or repaired. Therefore, no process monitoring and/or auxiliary heating elements during the deposition were used in the pilot implementation of this hybrid manufacturing approach. In addition, the materials selected for this study are typical for the production or repair of blades and/or blisks and other components operating in severe conditions. An axis symmetric Inconel718 substrate was utilised as a hub and CM247LC blades were deposited around its periphery at an even angular increment of 45° between them and thereafter machined/finished to dimension.

The hub (disk) was turned to diameter of 90 mm prior to the deposition operation utilising cutting parameters recommended for machining nickel-based superalloys, especially those recommended by the cutting tool manufacturer Sandvik® for their DNMG 15 06 12-SMR S05 F tools used in the study. The laser beam and powder cone were focused on the substrate's surface, while the deposition head and laser beam were maintained perpendicular to the surface throughout the deposition operation. The controller of the hybrid CNC machine manages the distance of the L-DED head from the axis of the cylindrical substrate to maintain the desired distance between the head and the substrate during the deposition process. The hub was preheated by defocusing the laser beam (the temperature was not monitored/recorded) and thus to minimise any warping and also to restrict the excessive heat draining from the deposition process to the substrate. Finally, the blades were finished by using WNT® cutting tools, i.e. 5,303,016,203, to remove a machining allowance of 0.3 mm at the periphery of the blades, while the cutting parameters used were those recommended by the manufacturer.

The CM247 LC blades were fabricated by using the parameters stated in Sect. 2.1, without any intermediate machining between the layers. This was done because it had a marginal effect on residual stresses, as discussed in Sect. 3.1.2, and also to minimise the processing time. The CM247 LC deposition regime discussed in Sect. 2.1 was deployed to build the blades up to a height of ~23 mm (2.4 cm³/blade). Then, a finish machining of the deposited structures was performed as it was found to introduce high compressive stresses and also to improve the surface integrity in general and the fatigue life of the AM structures as reported in literature [70].

The blades were built sequentially at 0, 90, 45, 180, 135, 225, 315, and 270°. This strategy was selected in order to achieve a sufficient heat flow between the multilayer blade depositions and the substrate, as it was already mentioned. Otherwise, the heat draining from the newly deposited blade to the previous ones could lead to an acute angle between the structures and very high solidification cracking and voids susceptibility [1, 71]. A typical structure suffering from such potential heat accumulation and draining between the blades is shown in Fig. 6, in spite of the fact that it was built utilising optimised process parameters for building dense walls free of cracks as reported earlier [43]. The figure indicates that the heat accumulation was excessive during the L-DED deposition and the nucleation of solidification cracks was enhanced [8]. On the contrary, the specially developed regime enhanced the cooling rates and consequently lowered the heat accumulation during the entire deposition process. Moreover, no macro-cracks were detected that reinforced further the benefits of using a dwelled deposition, complemented by sequential blade fabrication around the

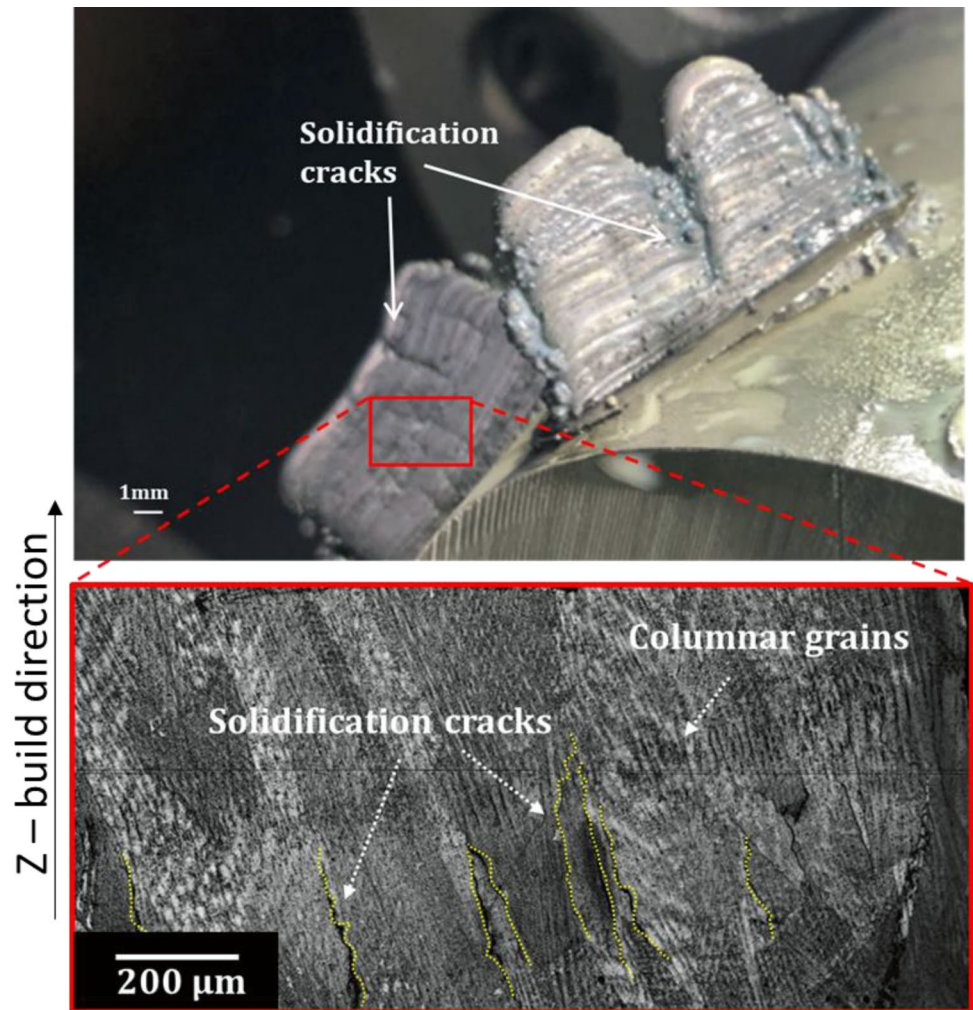
disk's periphery. The final blades manufactured utilising the bespoke regime were subsequently finished employing a side milling operation and it should be stressed, again, that this did not reveal any signs of cracks, as shown in Sect. 3.5.

In addition, the deposited structures in Fig. 6 confirm the role of a thick substrate in reducing the temperature within the first layers of deposition, thus acting as a heat sink. During the deposition of the adjacent layers, small cracks appeared at the bottom and subsequently more cracks propagated while additional layers were added. These cracks typically occur in the vicinity of the mushy zone where the material solidification is low. Especially, the cracks form when the temperature drops below the melting temperature, while the formed dendrites are typical vertically oriented for the L-DED process and follows the laser source towards the liquid phases in the interdendritic regions, according to Abdullah et al. [8]. Any remaining liquid regions acted as stress concentration and crack initiation sites while the relatively weak solid–liquid boundaries separate to an intergranular crack formation [72]. This result is confirmed by the cross-sectional image in Fig. 6, where vertically oriented intergranular solidification cracks nucleated parallel to the dendritic growth direction. Especially, the developed approach with the proposed dwelled deposition regime proved to be very successful in building blades of the defined height, free of macro or micro cracks.

3.3 Microstructure characterisation

Figure 7 depicts the microstructure at the cross section of a hybrid sample prior to the heat treatment. The elongated columnar dendritic microstructure at the deposited section and interface, growing towards the build direction, is typical for the material and the L-DED process. The microstructure at the interface area of the as-built part shows a high penetration rate in the $-Z$ direction towards the substrate, while no defects and minimal porosity can be observed. The interface of the as-built sample shows a high penetration and alternation of the microstructure and a columnar dendritic microstructure up to ~550 μm in the $-Z$ direction is dominant in the preform. This can be attributed to the CW laser source employed in the L-DED process. Especially, its effect on the deposited material and preform due to the induced significant fluid flow during the deposition defines the morphology of the melt pool and leads to a crack-free and nearly 100% density interface. The absence of cracks is in line with the results observed in Sect. 3.1, where the maximum principle stress is lower than the UTS and YS reported in the literature for L-DED and cast CM247LC, respectively [8, 63]. Apparently, the bottom of the microstructure at the interface consists of smaller grains compared to the subsequent layers. This is primarily related to the lower temperature of the preform,

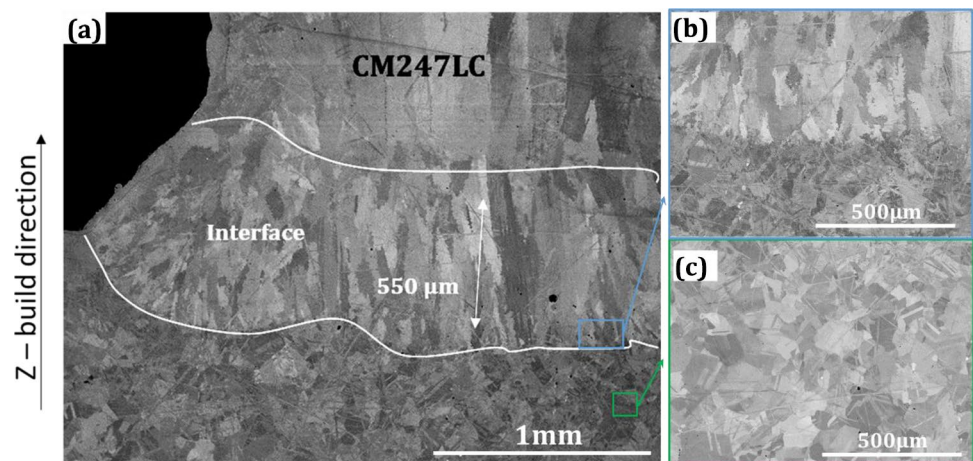
Fig. 6 Macro solidification cracks detected between the grain boundaries of the columnar dendrites on thin deposited walls



acting as a heat sink during the deposition that can lead to more equiaxed grains, as reported by Raghavan et al. [73]. According to Wang et al. [74], the grain growth at the fusion line (interface) or within the heat affected zone is limited due to the thermodynamic stability of the prior

coarser grains of the preform. Thus, the deposited material and the heat-affected zone below the interface exhibit the same microstructure that can be explained with the rapid solidification rates and the stimulating effect of the thick preform/substrate.

Fig. 7 Micrographs of as-built hybrid part showing microstructure in the X–Z plane: **a** the interface area between the deposited CM247LC and the substrate/preform; **b** a higher magnification image of the interface area; **c** the substrate microstructure



Below the heat affected zone, the Inconel preform exhibited the typical equiaxed grain structure with uniform grain size, without any signs of defects or segregations of laves phases in the microstructure, which could potentially arise from the laser-based AM process [75].

In the as-deposited section of the samples, layer bands are observed in the built section that are dominated by very tightly packed columnar dendrites, with a growth direction relative to that of the laser scanning direction as depicted in Fig. 8a. The evolution and presence of layer bands is dictated by the layer wise build strategy, especially the re-heating and re-melting cycles during the L-DED process. While the columnar growth of the dendrites is mainly due to the high temperature gradient as the consequence of the heat dissipation from the pre-deposited layers. According to literature, the laser scan direction influences the preferred growth direction in face-centred cubic materials such as CM247LC and Inconel718 during solidification. Therefore, a dendrite growth direction of $\sim 45^\circ$ is exhibited that is perpendicular to the prior deposited layer, as shown in Fig. 8 [76, 77]. The interdendritic region, as depicted in Fig. 8b and c, shows very small carbides. These regions are enriched in segregated elements leading to Hf carbides stabilisation [78]. Thus, the EDS analysis is not particularly significant, although, their formulation was studied extensively by other researchers, especially by Divya [79].

In CM247LC, extensive cracking can be explained with dislocations formed within the cells and at cell boundaries generated due to the high thermal stresses during the L-DED process. The blocking of dislocations may contribute to the extensive cracking of CM247LC since stresses generated during the deposition will increase if they cannot be relieved by glide or climb of dislocation [39]. Overall, the microstructure was free of cracks, and this is primarily associated with the high temperature during the process that enabled the formation of coarse grains. Their formation was followed by the rapid cooling rates, which was enhanced by the inter-layer dwell. The γ' phase was constrained to a submicron scale that led to a finer microstructure. The microstructural analysis, especially the absence of cracks, confirms again the low levels of stresses discussed in Sect. 3.1.

Notably, for the HT samples, the interface area shows a microstructural assimilation with the development of clearly equiaxed grains along the interface area, as per preform, while exhibiting a minimal porosity without any visible cracks or defects. The microstructural assimilation at the interface was associated with the topological arrangements during grain growth of the Inconel 718 due to the solution HT. The recrystallisation during the applied solution and temperature [62] results into the growth of larger equiaxed grains at the expense of smaller grains and thus stimulating the evolution of microstructure towards stable six-sided grains, curvature driven switching of neighbouring grains and shrinkage of three- and four-sided grains as depicted in Fig. 9a and b. This behaviour conforms to the experimental results reported for polycrystal materials by other studies, too [73]. It should be noted that the increase of the substrate grains size and refined equiaxed grain domination at the interface is proportional to the applied solution treatment time.

The Inconel 718 preform had equiaxed grains complemented by large dissolved segregated phases around the grain boundaries, mainly consisting of Nb and Ti, as shown by the EDS analysis in Fig. 10. The presence of Laves phases is quite known for cracks initiation and propagation and can have adverse effects on mechanical and fatigue properties of the material [48]. The heat treatments for the investigated material are studied extensively. In this work, the temperature of the solid solution step was selected to be above the solvus temperature of the Laves phase and long enough to dissolve the segregated phases into solution (Nb, Ti and Al). This is followed by ageing at two temperatures to grow the desired phases and harden the material (γ' and γ'') [48, 80]. Although, the selected HT regime dissolved the Laves phase and introduced the necessary hardening of the preform material, it did also introduce some minimal porosity at the interface and the grains of the preform as shown in Fig. 9. This could be possibly due to the expansion of entrapped gases and pores during the solution HT, generated from the L-DED process. Nevertheless, the absence of cracks and the intrinsic benefits to the microstructure and hardness for the hybrid sections confirm that the thermal post-treatment was

Fig. 8 Micrographs of as-built hybrid part depicting the CM247LC microstructure: **a** columnar grains; **b** high magnification image showing a dendritic structure; **c** higher magnification of an interdendritic region rich in carbides

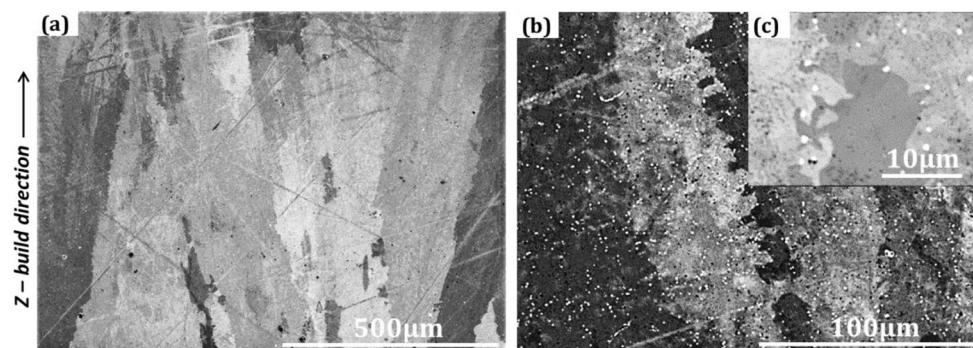




Fig. 9 Micrographs of the HT hybrid part: **a** the interface between the deposited structure and the substrate; **b** higher magnification image of the interface area; **c** the microstructure of the substrate

properly selected and adequate. However, it is worth noting that heat treatments were not optimised in this study.

The microstructure of the deposited section after the HT step is shown in Fig. 11 and appears more defined with distinguishable grain boundaries compared to the as-built sample. This phenomenon is related to the dissolution of the γ/γ' , after the solution HT and ageing at the specific temperature ranges. According to Wang et al. [39], the larger particles at the grain boundaries are formed during the solidification of γ' , while γ' in the centres are formed in the solid state from γ , the size of γ' is interlinked to the cooling rate, the eutectic temperature and γ' solvus.

The microstructure after the HT was free of cracks with an irregular morphology, thus confirming again the suitability of the temperature ranges selected for the solution HT. The microstructure exhibited intermittent grain boundaries that could possibly constrain any grain boundary sliding. The recrystallisation at 1200 °C forms large precipitates with a uniform size of $\sim 1 \mu\text{m}$. Cubic γ' is formed instead of the dendritic one at this temperature. Although, the size of the strengthening phase remained fine within the matrix due to the rapid air cooling during the solution and double ageing, thus suppressing any crack initiation which is consistent with other studies [81]. As can be seen in Fig. 11a, the γ' particles sides generally share the same orientation with the columnar grains giving often a sense of preferential orientation of the particles [78].

According to [82], the grains size and γ' particles inside the grain have a cuboidal morphology after a solution treatment ($> 1250 \text{ }^\circ\text{C}$) and ageing, with a size of approximately $1 \mu\text{m}$. Thus, as the temperature increases, the final γ' obtained is smaller and progressively with a higher volume fraction [78].

3.4 Hardness analysis

The hardness of hybrid samples in the interface area was investigated as it can be affected by both the L-DED process and the follow-up HT. Hardness tests were carried out at and near the interface to identify any hardness inconsistencies and thus to judge about the bonding quality and also in general about the mechanical properties of hybrid components. Especially, hardness tests were performed to reveal whether the deposition process altered the mechanical properties at and near the interface between the machined Inconel 718 preform/substrate and the L-DED CM247LC. The measurements were carried out on both, as-built and HT samples. As expected, the HT samples had a higher hardness compared to as-built ones. HT increased the hardness of as-deposited CM247LC, consistently, with 100HV near the interface as shown in Fig. 12b. The hardness evolution in the figure shows a lower hardness at the Inconel substrate compared to the deposited structure, which is in line with the hardness values reported in the literature for this material, in

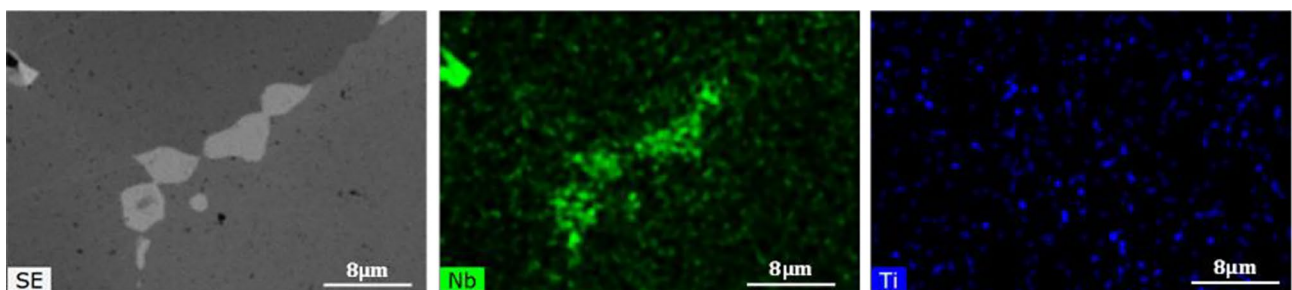


Fig. 10 EDS images of the solution at the substrate

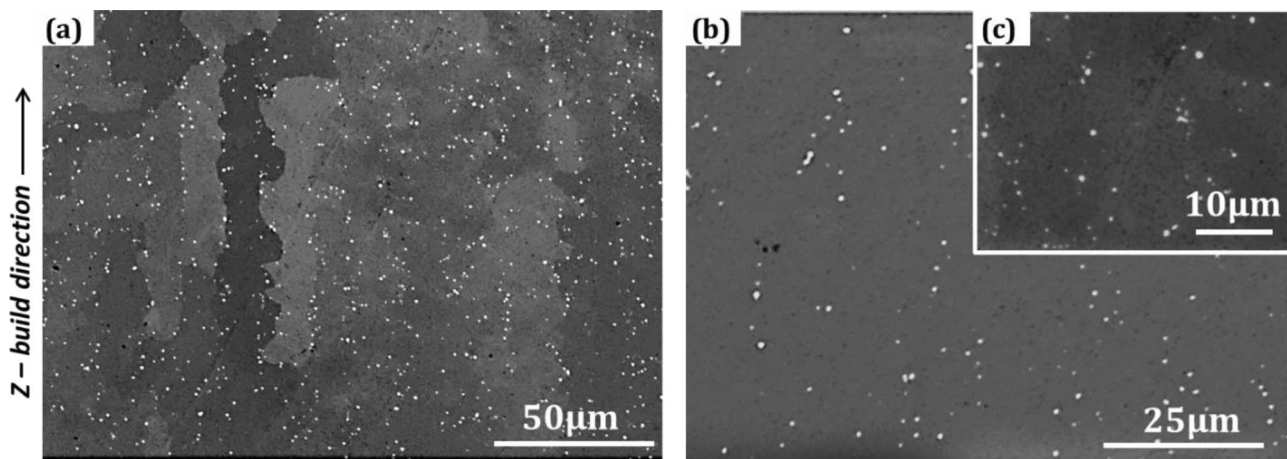


Fig. 11 Micrographs of HT part showing the microstructure of CM247LC: **a** the grain growth and orientation; **b** a high magnification image depict-

ing the microstructure homogenisation after HT; **c** a higher magnification image showing the grain boundaries with coarse and fine carbides

both conditions, although there is a trend for the hardness to increase instantly at the substrate near the interface, which can be explained with the microstructural assimilation and refinement at and near the interface as discussed in Sect. 3.3 and also the presence of high stresses at this area for the non-HT samples, while the hardness increased gradually for the HT samples, due to the recrystallisation, the stress relief and the grain coarsening occurring during the solution HT at the selected temperatures [62]. Concurrently, the increase of the substrate grains size and equiaxed grain domination at the interface after the HT explains the reduced hardness.

In particular, the interface area showed a microstructural assimilation through the development of equiaxed grains along the interface area as per the preform, as demonstrated in Sect. 3.3.

Overall, the obtained results prove that CM247LC can be L-DED deposited successfully on Inconel718 with a good bonding quality, hence resulting in good mechanical properties at the interface of hybrid components. The obtained hardness values are consistent to the ones reported in literature for both Inconel718 and CM247LC, for as-built and HT conditions, respectively [8, 50, 83].

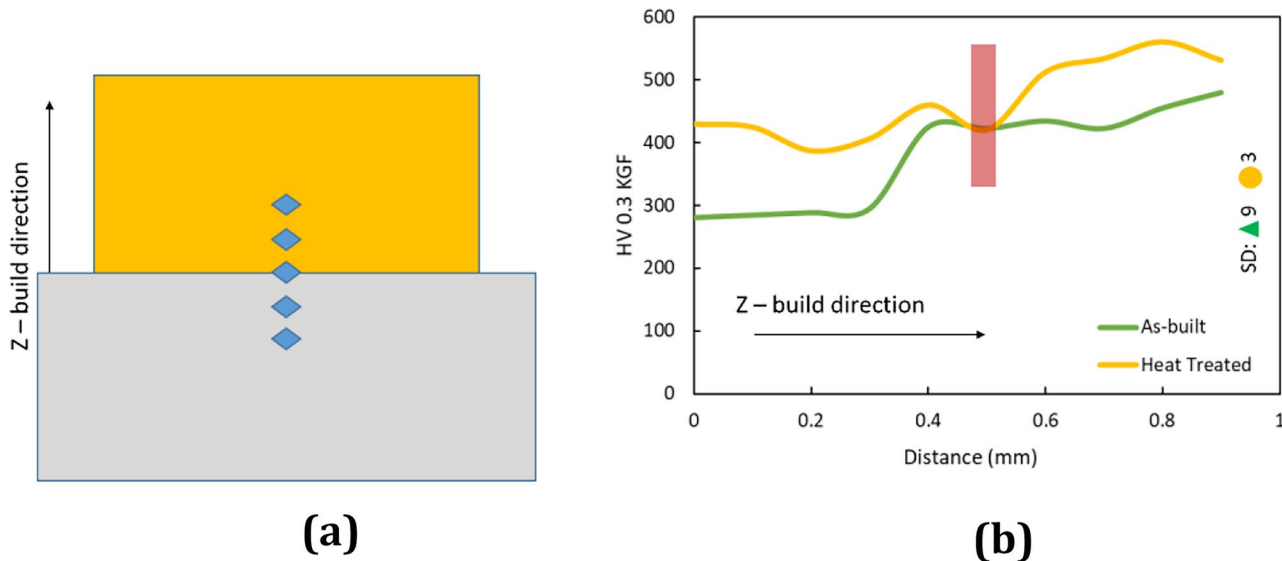


Fig. 12 The result of hardness tests: **a** a schematic of carried out hardness measurements; **b** the evolution of the hardness at and near the interface between the machined Inconel 718 substrate and the L-DED

deposited CM247LC from the two sets of hybrid cross sections measurements (the red vertical bar indicates the interface area, SD standard deviation)

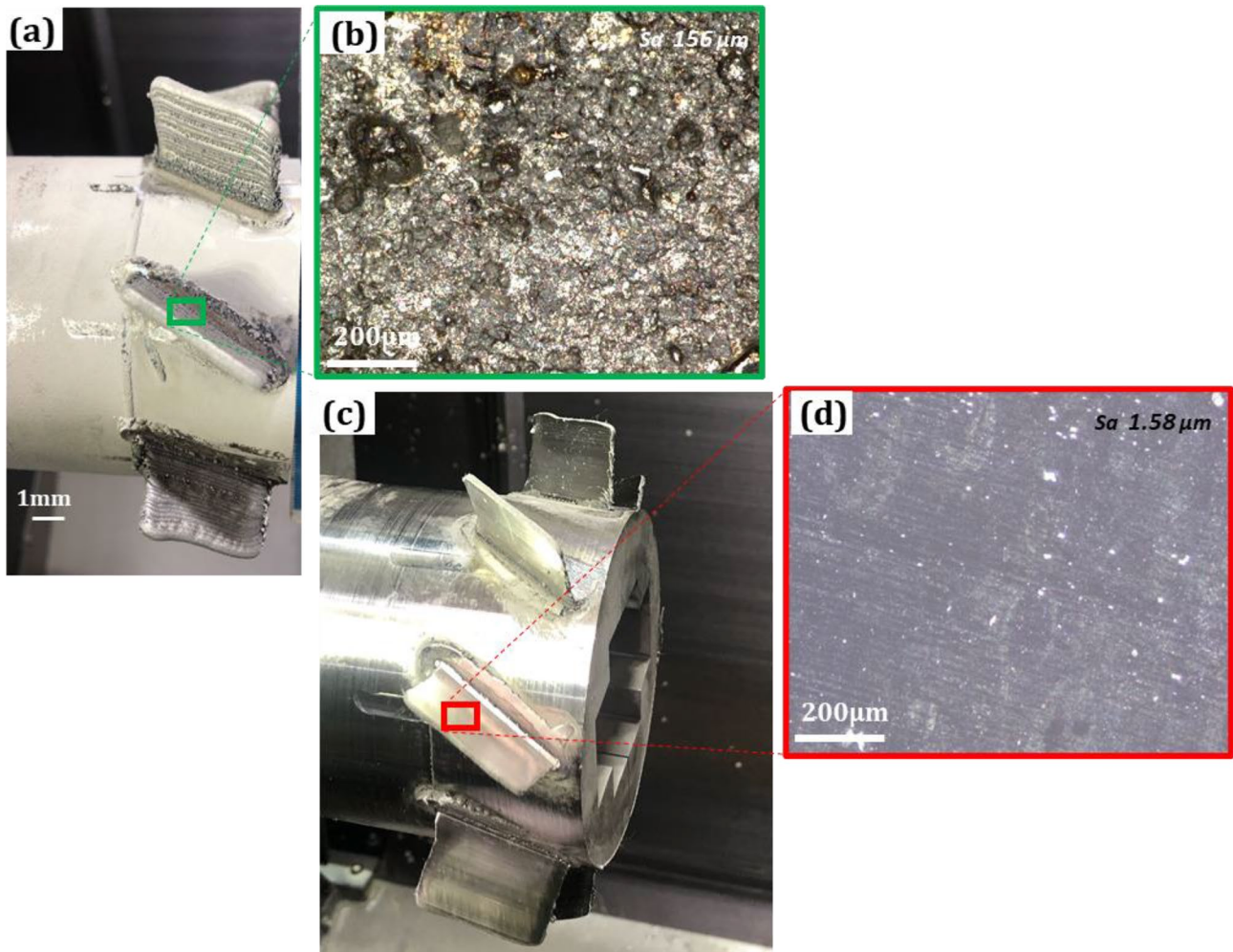


Fig. 13 A hybrid blisk demonstrator produced in a single hybrid processing setup: **a** and **c** the hybrid blisk before and after the finish machining produced using the specially developed L-DED regime that

is free of cracks; **b** and **d** micrographs of the surface before and after machining with the measured Sa roughness

3.5 Demonstrator part

Ultimately, a hybrid component was produced employing the L-DED technology. An Inconel 718 hub was machined and then CM247LC blades were built employing the specially developed L-DED deposition strategy (see Sect. 3.2) and subsequently finished by milling in a single setup as shown in Fig. 13. As all processing steps were completed in one setup, it was possible to maintain a higher processing accuracy with a minimum machining allowance for the finishing operation. As discussed earlier, no machining was performed before each deposition layer in this research, as the proposed deposition strategy delivered a crack free microstructure and low tensile residual stresses. The dimensions are indicative and were chosen only to prove that it is feasible to fabricate hybrid components made from two common nickel-based super alloys (Inconel718) and (CM247LC) on a

commercially available hybrid manufacturing machine tool, while minimising the processing time and cost.

4 Conclusions

The research reports a technology that can be applied to manufacture and repair of hybrid components from two common nickel-based super alloys, i.e. Inconel718 and CM247LC. A commercially available hybrid manufacturing machine tool was used in the experiments that integrates an AM process, i.e. L-DED, with a range of machining technologies. The results showed that a higher bonding performance at the interface between the two nickel-based alloys can be achieved, while the surface integrity was high without cracks and low tensile residual stresses. The following conclusions can be made based on the reported research results:

- The compressive stresses at the interface and into the machined substrate are reduced proportionally with each deposited layer. This is due to the thermal load induced during the L-DED process and the plastic deformations between layers that increase the tensile stresses. As the compressive stresses induced from machining remain unchanged, the final stress quotient at the interface is tensile.
- Inter-layer machining had a marginal impact on reducing residual stresses and the suppression of cracks compared to the inter-layer dwell and the finish machining of the deposited structures. In particular, the disrupted stress equilibrium from the machining, induced by the compressive stresses, is normalised after the L-DED layer-based deposition, while the benefits of the low thermal gradients between the processing area and the melting temperature remain. Therefore, the intermediate machining can be considered unnecessary and can be avoided to reduce the processing time and cost.
- Even though finish machining was reported to introduce compressive stresses to an adequate depth, heat treatments must be applied to the hybrid component to obtain the desired microstructure and an appropriate mechanical strength, and also to induce compressive residual stresses in and near the interface in the deposited CM247LC.
- Thicker preforms/substrates can have an adverse effect on the heat load during the L-DED process and therefore should be considered in determining the deposition parameters. Therefore, the optimised parameters should be used synergistically with other methods for minimising the thermal gradients during the deposition process and also between the substrate and the deposited structure. The deposition of defect free CM247LC blades on an Inconel 718 hub through L-DED can be achieved by applying an appropriate dwell and deposition strategy.
- The conducted investigation has confirmed that a sophisticated temperature control setup is not mandatory to achieve a CM247LC deposition free of cracks. Therefore, a conventional CNC machine tool with an integrated L-DED head can produce crack free AM structures with adequate mechanical properties.
- Low thermal gradients and fast cooling rates, enhanced by the interlayer dwell, can reduce the residual stresses into the deposited structures. Especially, the resulting tensile residual stresses can be significantly lower than the UTS and YS values reported for as-cast, L-PBF and L-DED structures, respectively. Notably, the internal strain did not exceed the CM247LC ductility and therefore no crack formation had been triggered. If measures are not taken to reduce the thermal gradient, it could lead to delamination between the substrate and the deposited section, at the interface, though this could be suppressed through substrate pre-heating and inter-layer dwell, as

observed through the hardness and microstructural analysis of the interface.

- The CW laser was found to have a significant effect onto the microstructure, perpendicular to its scan direction. Especially, the CW laser was able to create a microstructural assimilation between the Inconel 718 substrate and the deposited CM247LC up to a depth of ~ 0.5 mm and thus establishing a strong metallurgical bonding. In addition, a heat treatment can be selected to dissolve any segregated phases in the substrate and trigger the growth of the desired hardening phases. The recrystallisation induced growth of larger equiaxed grains and the microstructural assimilation at the interface can improve further the metallurgical bonding.
- A continuous pre-heating to control the CM247LC solidification cracking at the temperature ranges reported in literature could have a significant negative impact onto the Inconel 718 microstructure, when depositing structures on Inconel 718 substrates/preforms. However, by applying the proposed approach to control the thermal gradients during L-DED in this research, it was possible to produce crack free CM247LC structures with good interface bonding, strength and microstructure for as-built and heat-treated conditions.

Appendix

Sample preparation for residual stress analysis

The substrate used for the preparation of the residual stress specimen was a solid cylinder with a $\Phi 19$ diameter and height of 30 mm. CM247LC was deposited at the cross section of the preform in XY plane with a diameter very similar to that of the preform and a height of ~ 9 mm in the Z+ direction (2.5 cm^3).

Face milling was conducted with a $\Phi 16$ solid-cemented carbide slotting cutter, manufactured and supplied by WNT tools ID 50 967 16,220. The process parameters recommended by manufacturer were employed. Face milling was applied onto the planar area of each substrate, before the deposition to ensure its flatness. In addition, intermediate milling was applied after every 4 deposition layers (~ 5 mm) on selected samples, to investigate the effects of inter-layer machining onto the residual stresses. The intermediate machining was limited to three passes of 0.1 mm axial depth, to maintain the processing time low and maximise the tool life. Prior to any material deposition, a pre-heating of the substrate was performed with the laser (no powder was deposited during this stage), to mitigate the effects of the thermal shock. Especially, this allowed a low

temperature gradient to be maintained and subsequently to reduce the stress accumulation between the substrate and deposited structures, during the L-DED process. Preheating cycles are reported in literature to reduce effectively the residual stresses and cooling rate in pre heated powder bed. The preheating was conducted through the integrated CW laser source into the machine and thus to keep the setup as simple as possible. This approach proved to be beneficial and can be applied for the pre-heating components in case of a rethreading process, such as the repair of a blade or disk, although, the pre-heat temperature was not recorded.

For simplification, the main symbols and their meaning are listed in Table 3.

Milling Parameters	
ae	Milling width 30%
ap	Milling depth 0.1mm x3 passes
t	Milling thickness
Vc	Cutting speed 25m/min

Three sets of hybrid samples were prepared in this research: (1) as-built condition; (2) intermediate machining and (3) intermediate machining + solution HT, and double ageing.

The L-DED process used to produce the hybrid components was carried out by alternating milling and deposition every ~5 mm. As shown in Fig. 14 (rough example), a spiral deposition strategy, starting from the centre, with a constant feed rate of 240 mm/min was selected. The aim was to minimise the residual stresses induced into the sample during the deposition and also to control the temperature gradient inside the part, by eliminating any laser power interruption [84].

Target gauge/centre hole drilling method via deep hole drilling (DHD) was employed to assess the residual stresses. The measurements were taken at the top planar face of the

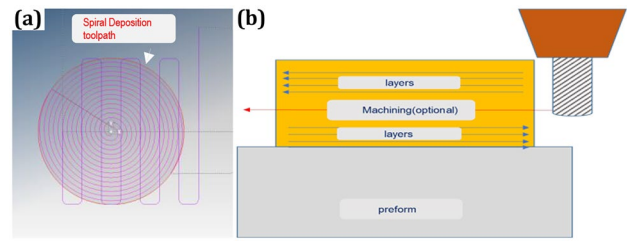


Fig. 14 Schematic representation of the deposition strategy with the intermediate layers and then machining was conducted to prepare samples for the residual stresses analysis: (a) depicts a spiral material deposition toolpath, with a subsequent machining process; (b) shows the unidirectional deposition strategy together with machining strategy, i.e. toolpath selected for the intermediately machined layers (rough example)

deposited structure where the gauge was attached onto the flat face of the deposited material, and a second gauge was attached on the outside diameter (OD) of the substrate.

Figure 15 shows a representative cross section of a hybrid sample in XZ plane. The microstructural variations between the preform section and the deposited CM247LC section, can be seen as well as the interface area where the welding between the two sections occurs. This observation was required in order to determine the location for the strain gauge attachment at the interface for the subsequent residual stress measurement.

Notably, the microstructural assimilation between the two materials, at the interface, appears to be greater than 450 µm with some minimal porosity into the deposited section of the as-built sample (the microstructure of the hybrid components). Figure 15(a) shows tilted welds to the substrate. The unevenness is not related to the substrate because machining cycle was performed to ensure the flatness of the substrate prior to the deposition. It is therefore considered to be related to the flatness of the machine workholding setup

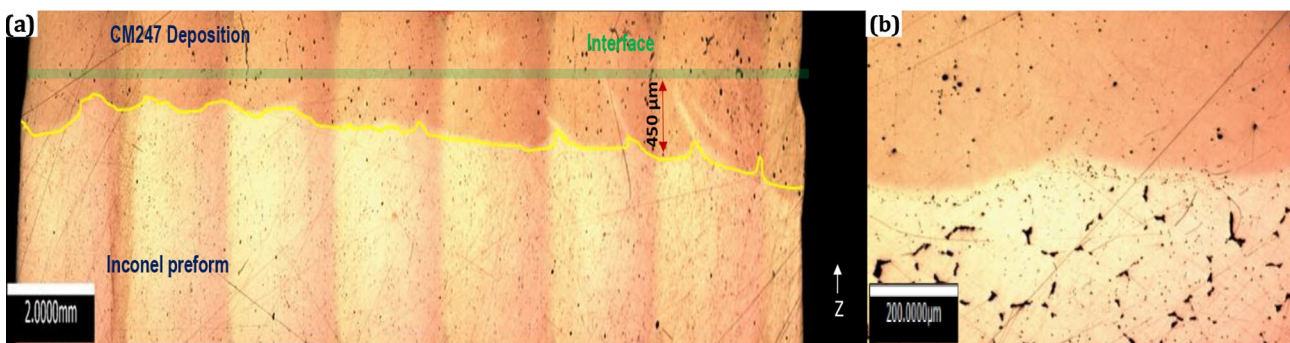


Fig. 15 Micrographs of a representative hybrid sample cross section: (a) shows the material deposition boundaries, with the interface region and the heat affected zone of an as built sample. Translucent bar depicts the interface region, while yellow curve presents the boundaries of the heat affected zone between the interface and the preform,

with a penetration depth of ~450 µm in the -Z direction; (b) shows a higher magnification micrograph of a HT sample where the preform and deposited structure can be seen together with a defined interface region

where the samples were held and/or the acute angle occurring during the heat draining.

Apparently, one or two layers of material onto the substrate were re-melt or weld throughout the few first layers of the L-DED process. This could potentially affect the mechanical properties. Therefore, the welding at the machined preform was evaluated through a hardness analysis to investigate its impact at the interface.

Author contribution Not applicable.

Funding This study was funded by the ESPRC grant (EP/M507672/1) and the ERDF “Smart Factory Hub” (SmartFub) projects and the Manufacturing Technology Centre (MTC) for the financial support of Aldi Mehmeti’s Ph.D. research.

Availability of data and materials All data generated or analysed during this study are included in this article.

Code availability Not applicable.

Declarations

Ethics approval This paper is our original unpublished work, and it has not been submitted to any other journal for reviews.

Consent to participate All authors were fully involved in the study and preparation of the manuscript, each of the authors has read and concurs with the content in the final manuscript.

Consent for publication All authors consent to publish the content in the final manuscript.

Competing interests The authors declare no competing interests.

Open Access This article is licensed under a Creative Commons Attribution 4.0 International License, which permits use, sharing, adaptation, distribution and reproduction in any medium or format, as long as you give appropriate credit to the original author(s) and the source, provide a link to the Creative Commons licence, and indicate if changes were made. The images or other third party material in this article are included in the article’s Creative Commons licence, unless indicated otherwise in a credit line to the material. If material is not included in the article’s Creative Commons licence and your intended use is not permitted by statutory regulation or exceeds the permitted use, you will need to obtain permission directly from the copyright holder. To view a copy of this licence, visit <http://creativecommons.org/licenses/by/4.0/>.

References

- Kaierle S, Overmeyer L, Alfred I et al (2017) Single-crystal turbine blade tip repair by laser cladding and remelting. *CIRP J Manuf Sci Technol* 19:196–199. <https://doi.org/10.1016/J.CIRPJ.2017.04.001>
- Shrivastava A, Anand Kumar S, Rao S et al (2021) Remanufacturing of nickel-based aero-engine components using metal additive manufacturing technology. *Mater Today Proc* 45:4893–4897. <https://doi.org/10.1016/J.MATPR.2021.01.355>
- Gas Turbine Engineering Handbook - Meherwan P. Boyce - Google Books
- Mishra RK, Thomas J, Srinivasan K et al (2017) Failure analysis of an un-cooled turbine blade in an aero gas turbine engine. *Eng Fail Anal* 79:836–844. <https://doi.org/10.1016/J.ENGFAILANAL.2017.05.042>
- Biermann H, Ungár T, von Grossmann B, Mechsner S (2004) Microbeam synchrotron radiation diffraction study of local strains in a monocrystalline nickel-base turbine blade. *Mater Sci Eng A* 387–389:918–922. <https://doi.org/10.1016/J.MSEA.2004.01.081>
- Wang C, Shi D, Yang X et al (2017) An improved viscoplastic constitutive model and its application to creep behavior of turbine blade. *Mater Sci Eng A* 707:344–355. <https://doi.org/10.1016/J.MSEA.2017.09.067>
- Caruso S, Imbrogno S, Rotella G et al (2015) Numerical simulation of surface modification during machining of nickel-based superalloy. *Procedia CIRP* 31:130–135. <https://doi.org/10.1016/J.PROCIR.2015.03.053>
- Alhuzaim A, Imbrogno S, Attallah MM (2021) Direct laser deposition of crack-free CM247LC thin walls: mechanical properties and microstructural effects of heat treatment. *Mater Des*. <https://doi.org/10.1016/J.MATDES.2021.110123>
- Ulutan D, Ozel T (2011) Machining induced surface integrity in titanium and nickel alloys: a review. *Int J Mach Tools Manuf* 51:250–280
- Axinte DA, Andrews P, Li W et al (2006) Turning of advanced Ni based alloys obtained via powder metallurgy route. *CIRP Ann* 55:117–120. [https://doi.org/10.1016/S0007-8506\(07\)60379-5](https://doi.org/10.1016/S0007-8506(07)60379-5)
- Wong CN, Huang HZ, Li N (2013) Fourier series based reliability analysis of aeroengine turbine blade under linear fuzzy safety state. *Eng Fail Anal* 31:268–280. <https://doi.org/10.1016/J.ENGFAILANAL.2013.02.007>
- Dong YW, Li XL, Zhao Q et al (2017) Modeling of shrinkage during investment casting of thin-walled hollow turbine blades. *J Mater Process Technol* 244:190–203. <https://doi.org/10.1016/J.JMATPROTEC.2017.01.005>
- Liu C, Jin S, Lai X et al (2014) (2014) Influence of complex structure on the shrinkage of part in investment casting process. *Int J Adv Manuf Technol* 775(77):1191–1203. <https://doi.org/10.1007/S00170-014-6523-Y>
- Kounitzky A, Wortmann J, Agarwal PN (1991) A single crystal casting process for high-temperature components. *Mater Des* 12:323–330. [https://doi.org/10.1016/0261-3069\(91\)90074-E](https://doi.org/10.1016/0261-3069(91)90074-E)
- Smallman RE, Ngan AHW (2013) Directional solidification modern physical metallurgy: eighth edition. In: *Modern Physical Metallurgy: Eighth Edition, Eighth Edition*. Elsevier Inc., pp 1–697
- Carter LN, Essa K, Attallah MM (2015) Optimisation of selective laser melting for a high temperature Ni-superalloy. *Rapid Prototyp J* 21:423–432. <https://doi.org/10.1108/RPJ-06-2013-0063/FULL/PDF>
- Quan Z, Wu A, Keefe M et al (2015) Additive manufacturing of multi-directional preforms for composites: opportunities and challenges. *Mater Today* 18:503–512. <https://doi.org/10.1016/J.MATTOD.2015.05.001>
- Wang X, Carter LN, Adkins NJE et al (2020) Novel hybrid manufacturing process of CM247LC and multi-material blisks. *Micromachines*. <https://doi.org/10.3390/M11050492>
- Shah P, Racasan R, Bills P (2016) Comparison of different additive manufacturing methods using computed tomography. *Case Stud Nondestruct Test Eval* 6:69–78. <https://doi.org/10.1016/J.CSNDT.2016.05.008>
- Xu Z, Hyde CJ, Tuck C, Clare AT (2018) Creep behaviour of inconel 718 processed by laser powder bed fusion. *J Mater Process Technol* 256:13–24. <https://doi.org/10.1016/J.JMATPROTEC.2018.01.040>

21. Wang D, Li S, Deng G et al (2021) A melt pool temperature model in laser powder bed fabricated CM247LC Ni superalloy to rationalize crack formation and microstructural inhomogeneities. *Metall Mater Trans A* 2021:1–14. <https://doi.org/10.1007/S11661-021-06457-5>
22. Wang X (2018) Improving the microstructure, mechanical properties & process route in selective laser melting of nickel-superalloys
23. Gorsse S, Hutchinson C, Gouné M, Banerjee R (2017) Additive manufacturing of metals: a brief review of the characteristic microstructures and properties of steels, Ti-6Al-4V and high-entropy alloys. <https://doi.org/10.1080/14686996.2017.1361305>
24. Seifi M, Salem A, Beuth J et al (2016) (2016) Overview of materials qualification needs for metal additive manufacturing. *JOM* 68(3):747–764. <https://doi.org/10.1007/S11837-015-1810-0>
25. Polonsky AT, Echlin MP, Lenthe WC et al (2018) Defects and 3D structural inhomogeneity in electron beam additively manufactured Inconel 718. *Mater Charact* 143:171–181. <https://doi.org/10.1016/J.MATCHAR.2018.02.020>
26. Li S, Zhuang J, Yang J, et al The effect of delta-phase on crack propagation under creep and fatigue conditions in alloy 718
27. González H, Pereira O, de Lacalle LNL et al (2021) Flank-milling of integral blade rotors made in Ti6Al4V using Cryo CO2 and minimum quantity lubrication. *J Manuf Sci Eng Trans ASME*. <https://doi.org/10.1115/1.4050548/1104369>
28. Calleja A, González H, Polvorosa R et al (2019) Blisk blades manufacturing technologies analysis. *Procedia Manuf* 41:714–722. <https://doi.org/10.1016/J.PROMFG.2019.09.062>
29. Klocke F, Schmitt R, Zeis M et al (2015) Technological and economical assessment of alternative process chains for blisk manufacture. *Procedia CIRP* 35:67–72. <https://doi.org/10.1016/J.PROCIR.2015.08.052>
30. Blakey-Milner B, Gradl P, Snedden G et al (2021) Metal additive manufacturing in aerospace: a review. *Mater Des* 209:110008. <https://doi.org/10.1016/J.MATDES.2021.110008>
31. Penchev P, Bhaduri D, Dimov S, Soo S (2014) Novel manufacturing platform for scale up production of miniaturized parts. 231–238
32. Flynn JM, Shokrani A, Newman ST, Dhokia V (2016) Hybrid additive and subtractive machine tools – research and industrial developments. *Int J Mach Tools Manuf* 101:79–101. <https://doi.org/10.1016/J.IJMACHTOOLS.2015.11.007>
33. LASERTEC 65 3D – Additive Manufacturing in milling quality. <https://uk.dmgmori.com/news-and-media/technical-press-news/news/lasertec-65-3d-additive-manufacturing-in-milling-quality>. Accessed 12 Jul 2021
34. Merklein M, Junker D, Schaub A, Neubauer F (2016) Hybrid additive manufacturing technologies – an analysis regarding potentials and applications. *Phys Procedia* 83:549–559. <https://doi.org/10.1016/J.PHPRO.2016.08.057>
35. Pereira JC, Zubiri F, Garmendia MJ et al (2022) Study of laser metal deposition additive manufacturing, CNC milling, and NDT ultrasonic inspection of IN718 alloy preforms. *Int J Adv Manuf Technol* 120:2385–2406. <https://doi.org/10.1007/S00170-022-08905-X/TABLES/6>
36. Chen L, Mi G, Zhang X, Wang C (2019) Numerical and experimental investigation on microstructure and residual stress of multi-pass hybrid laser-arc welded 316L steel. *Mater Des* 168:107653. <https://doi.org/10.1016/J.MATDES.2019.107653>
37. Denny J, Jinoop AN, Paul CP et al (2020) Fatigue crack propagation behaviour of inconel 718 structures built using directed energy deposition based laser additive manufacturing. *Mater Lett*. <https://doi.org/10.1016/j.matlet.2020.128241>
38. Sidhu RK, Ojo OA (2008) Chaturvedi MC (2008) Microstructural response of directionally solidified René 80 superalloy to gas-tungsten arc welding. *Metall Mater Trans A* 40(14):150–162. <https://doi.org/10.1007/S11661-008-9700-5>
39. Wang X, Carter LN, Pang B et al (2017) Microstructure and yield strength of SLM-fabricated CM247LC Ni-superalloy. *Acta Mater* 128:87–95. <https://doi.org/10.1016/j.actamat.2017.02.007>
40. Muñoz-Moreno R, Divya VD, Driver SL et al (2016) Effect of heat treatment on the microstructure, texture and elastic anisotropy of the nickel-based superalloy CM247LC processed by selective laser melting. *Mater Sci Eng A* 674:529–539. <https://doi.org/10.1016/J.MSEA.2016.06.075>
41. Seidel A, Finaske T, Straubel A et al (2018) (2018) Additive manufacturing of powdery Ni-based superalloys Mar-M-247 and CM 247 LC in hybrid laser metal deposition. *Metall Mater Trans A* 49(49):3812–3830. <https://doi.org/10.1007/S11661-018-4777-Y>
42. Bidron G, Doghri A, Malot T et al (2020) Reduction of the hot cracking sensitivity of CM-247LC superalloy processed by laser cladding using induction preheating. *J Mater Process Technol* 277:116461. <https://doi.org/10.1016/J.JMATPROTEC.2019.116461>
43. Bidare P, Mehmeti A, Jiménez A et al (2022) High-density direct laser deposition (DLD) of CM247LC alloy: microstructure, porosity and cracks. *Int J Adv Manuf Technol* 120:8063–8074. <https://doi.org/10.1007/S00170-022-09289-8/FIGURES/13>
44. Yamazaki T (2016) Development of a hybrid multi-tasking machine tool: integration of additive manufacturing technology with CNC machining. *Procedia CIRP* 42:81–86. <https://doi.org/10.1016/J.PROCIR.2016.02.193>
45. Desvallées Y, Bouzidi M, Bois F, Beaudé N Delta phase in Inconel 718: mechanical properties and forging process requirements
46. Moradi M, Hasani A, Malekshahi Beiranvand Z, Ashoori A (2020) Additive manufacturing of stellite 6 superalloy by direct laser metal deposition – part 2: effects of scanning pattern and laser power reduction in different layers. *Opt Laser Technol* 131:106455. <https://doi.org/10.1016/J.OPTLASTEC.2020.106455>
47. Zhao X, Dong S, Yan S et al (2020) The effect of different scanning strategies on microstructural evolution to 24CrNiMo alloy steel during direct laser deposition. *Mater Sci Eng A* 771:138557. <https://doi.org/10.1016/J.MSEA.2019.138557>
48. Kouraytem N, Varga J, Amin-Ahmadi B et al (2021) A recrystallization heat-treatment to reduce deformation anisotropy of additively manufactured Inconel 718. *Mater Des* 198:109228. <https://doi.org/10.1016/J.MATDES.2020.109228>
49. Boswell JH, Clark D, Li W, Attallah MM (2019) Cracking during thermal post-processing of laser powder bed fabricated CM247LC Ni-superalloy. *Mater Des* 174:107793. <https://doi.org/10.1016/J.MATDES.2019.107793>
50. Careri F, Imbrogno S, Umbrello D et al (2021) Machining and heat treatment as post-processing strategies for Ni-superalloys structures fabricated using direct energy deposition. *J Manuf Process* 61:236–244. <https://doi.org/10.1016/J.JMAPRO.2020.11.024>
51. Carranza RM (2020) Determination of residual stress in components manufactured using laser powder bed fusion (L-PBF)
52. Anderson LS, Venter AM, Vrancken B, et al (2018) Investigating the residual stress distribution in selective laser melting produced Ti-6Al-4V using neutron diffraction. *Mater Res Proc* 4:73–78. <https://doi.org/10.21741/9781945291678-11>
53. Mehmeti A, Lynch D, Penchev P (2021) The effect of hot isostatic pressing on surface integrity, microstructure and strength of hybrid metal injection moulding, and laser-based powder bed fusion stainless-steel components. *Appl Sci*, et al 2021 11 7490. <https://doi.org/10.3390/APP11167490>
54. Vasinonta A, Beuth JL, Griffith M (2007) Process maps for predicting residual stress and melt pool size in the laser-based fabrication of thin-walled structures. *J Manuf Sci Eng* 129:101–109. <https://doi.org/10.1115/1.2335852>
55. Gusarov AV, Pavlov M, Smurov I (2011) Residual stresses at laser surface remelting and additive manufacturing. *Phys Procedia* 12:248–254. <https://doi.org/10.1016/J.PHPRO.2011.03.032>

56. Mehmeti A, Penchev P, Lynch D et al (2020) Mechanical behaviour and interface evaluation of hybrid MIM/PBF stainless steel components. *Rapid Prototyp J* 26:1809–1825. <https://doi.org/10.1108/RPJ-10-2019-0256>
57. Fuhrich T, Berger P, Hügel H (2001) Marangoni effect in laser deep penetration welding of steel. *J Laser Appl* 13:178. <https://doi.org/10.2351/1.1404412>
58. Guo C, Zhou Y, Li X et al (2021) A comparing study of defect generation in IN738LC superalloy fabricated by laser powder bed fusion: continuous-wave mode versus pulsed-wave mode. *J Mater Sci Technol* 90:45–57. <https://doi.org/10.1016/J.JMST.2021.03.006>
59. Zhong C, Gasser A, Schopphoven T, Poprawe R (2015) Experimental study of porosity reduction in high deposition-rate laser material deposition. *Opt Laser Technol* 75:87–92. <https://doi.org/10.1016/J.OPTLASTEC.2015.06.016>
60. Alhuzaim A, Imbrogno S, Attallah MM (2021) Controlling microstructural and mechanical properties of direct laser deposited Inconel 718 via laser power. *J Alloys Compd* 872:159588. <https://doi.org/10.1016/J.JALLCOM.2021.159588>
61. Barros R, Silva FJG, Gouveia RM (2019) Laser powder bed fusion of Inconel 718: residual stress analysis before and after heat treatment. *Met*, et al. 9 1290. <https://doi.org/10.3390/MET9121290>
62. Tucho WM, Cuvillier P, Sjolyst-Kverneland A, Hansen V (2017) Microstructure and hardness studies of Inconel 718 manufactured by selective laser melting before and after solution heat treatment. *Mater Sci Eng A* 689:220–232. <https://doi.org/10.1016/J.MSEA.2017.02.062>
63. Kim IS, Choi BG, Hong HU et al (2011) Anomalous deformation behavior and twin formation of Ni-base superalloys at the intermediate temperatures. *Mater Sci Eng A* 528:7149–7155. <https://doi.org/10.1016/J.MSEA.2011.05.083>
64. Denlinger ER, Heigel JC, Michaleris P, Palmer TA (2015) Effect of inter-layer dwell time on distortion and residual stress in additive manufacturing of titanium and nickel alloys. *J Mater Process Technol* 215:123–131. <https://doi.org/10.1016/J.JMATPROTEC.2014.07.030>
65. Fessler JR, Merz R, Nickel A et al (1996) Laser deposition of metals for shape deposition manufacturing. <https://doi.org/10.15781/T29Z90X7D>
66. Kadrigama K, Abu Bakar R, Rahman M, Mohamad B Modeling of residual stress
67. Imbrogno S, Rinaldi S, Umbrello D et al (2018) A physically based constitutive model for predicting the surface integrity in machining of Waspaloy. *Mater Des* 152:140–155. <https://doi.org/10.1016/J.MATDES.2018.04.069>
68. Madariaga A, Kortabarria A, Hormaetxe E et al (2016) Influence of tool wear on residual stresses when turning Inconel 718. *Procedia CIRP* 45:267–270. <https://doi.org/10.1016/J.PROCIR.2016.02.359>
69. Shah K, Haq IU, Shah SA et al (2014) Experimental study of direct laser deposition of ti-6al-4v and inconel 718 by using pulsed parameters. *Sci World J*. <https://doi.org/10.1155/2014/841549>
70. Sasahara H (2005) The effect on fatigue life of residual stress and surface hardness resulting from different cutting conditions of 0.45%C steel. *Int J Mach Tools Manuf* 45:131–136. <https://doi.org/10.1016/J.IJMACHTOOLS.2004.08.002>
71. Rottwinkel B, Pereira A, Alfred I et al (2017) Turbine blade tip single crystalline clad deposition with applied remelting passes for well oriented volume extension. *J Laser Appl* 29:022310. <https://doi.org/10.2351/1.4983667>
72. Dye D, Hunziker O, Reed RC (2001) Numerical analysis of the weldability of superalloys. *Acta Mater* 49:683–697. [https://doi.org/10.1016/S1359-6454\(00\)00361-X](https://doi.org/10.1016/S1359-6454(00)00361-X)
73. Raghavan S, Sahay SS (2007) Modeling the grain growth kinetics by cellular automaton. *Mater Sci Eng A* 445–446:203–209. <https://doi.org/10.1016/J.MSEA.2006.09.023>
74. Wang T, Zhu YY, Zhang SQ et al (2015) Grain morphology evolution behavior of titanium alloy components during laser melting deposition additive manufacturing. *J Alloys Compd* 632:505–513. <https://doi.org/10.1016/j.jallcom.2015.01.256>
75. Oliveira JP, Santos TG, Miranda RM (2020) Revisiting fundamental welding concepts to improve additive manufacturing: from theory to practice. *Prog Mater Sci* 107:100590. <https://doi.org/10.1016/J.PMATSCI.2019.100590>
76. Li S, Xiao H, Liu K et al (2017) Melt-pool motion, temperature variation and dendritic morphology of Inconel 718 during pulsed- and continuous-wave laser additive manufacturing: a comparative study. *Mater Des* 119:351–360. <https://doi.org/10.1016/J.MATDES.2017.01.065>
77. Dinda GP, Dasgupta AK, Mazumder J (2012) Texture control during laser deposition of nickel-based superalloy. *Scr Mater* 67:503–506. <https://doi.org/10.1016/J.SCRIPTAMAT.2012.06.014>
78. Bassini E, Sivo A, Martelli PA et al (2022) Effects of the solution and first aging treatment applied to as-built and post-HIP CM247 produced via laser powder bed fusion (LPBF). *J Alloys Compd* 905:164213. <https://doi.org/10.1016/J.JALLCOM.2022.164213>
79. Divya VD, Muñoz-Moreno R, Messé OMDM et al (2016) Microstructure of selective laser melted CM247LC nickel-based superalloy and its evolution through heat treatment. *Mater Charact* 114:62–74. <https://doi.org/10.1016/J.MATCHAR.2016.02.004>
80. Calandri M, Manfredi D, Calignano F et al (2018) Solution treatment study of Inconel 718 produced by SLM additive technique in view of the oxidation resistance. *Adv Eng Mater* 20:1800351. <https://doi.org/10.1002/ADEM.201800351>
81. Saito T, Chen YT, Takata Y (2020) Effect of heat treatments on the microstructural evolution of a single crystal high-entropy superalloy. *Met*, et al. 10 1600. <https://doi.org/10.3390/MET10121600>
82. MacDonald JE (2017) Hot isostatic pressing of a high temperature Ni-superalloy CM247LC : processing-microstructure-properties
83. McNutt PA (2015) An investigation of cracking in laser metal deposited nickel superalloy CM247LC
84. Yeung H, Chen J, Yang G et al (2021) Effect of spiral scan strategy on microstructure for additively manufactured stainless steel 17–4. *Manuf Lett* 29:1–4. <https://doi.org/10.1016/J.MFGLET.2021.04.005>

Publisher's Note Springer Nature remains neutral with regard to jurisdictional claims in published maps and institutional affiliations.